On Air–Sea Interaction at the Mouth of the Gulf of California

PAQUITA ZUIDEMA
Rosenstiel School of Marine and Atmospheric Sciences, University of Miami, Miami, Florida

CHRIS FAIRALL
NOAA/Earth System Research Laboratory/Physical Sciences Division, Boulder, Colorado

LESLIE M. HARTTEN AND JEFFREY E. HARE
NOAA/Earth System Research Laboratory, and CIRES Climate Diagnostics Center, University of Colorado, Boulder, Colorado

DANIEL WOLFE
NOAA/Earth System Research Laboratory/Physical Sciences Division, Boulder, Colorado

(Manuscript received 6 December 2005, in final form 16 June 2006)

ABSTRACT

Surface flux, wind profiler, oceanic temperature and salinity, and atmospheric moisture, cloud, and wind observations gathered from the R/V *Altair* during the North American Monsoon Experiment (NAME) are presented. The vessel was positioned at the mouth of the Gulf of California halfway between La Paz and Mazatlan (~23.5°N, 108°W), from 7 July to 11 August 2004, with a break from 22 to 27 July. Experiment-mean findings include a net heat input from the atmosphere into the ocean of 70 W m^{-2}. The dominant cooling was an experiment-mean latent heat flux of 108 W m^{-2}, equivalent to an evaporation rate of 0.16 mm h^{-1}. Total accumulated rainfall amounted to 42 mm. The oceanic mixed layer had a depth of approximately 20 m and both warmed and freshened during the experiment, despite a dominance of evaporation over local precipitation. The mean atmospheric boundary layer depth was approximately 410 m, deepening with time from an initial value of 350 m. The mean near-surface relative humidity was 66%, increasing to 73% at the top of the boundary layer. The rawinsondes documented an additional moist layer between 2- and 3-km altitude associated with a land–sea breeze, and a broad moist layer at 5–6 km associated with land-based convective outflow. The observational period included a strong gulf surge around 13 July associated with the onset of the summer monsoon in southern Arizona. During this surge, mean 1000–700-hPa winds reached 12 m s^{-1}, net surface fluxes approached zero, and the atmosphere moistened significantly but little rainfall occurred. The experiment-mean wind diurnal cycle was dominated by mainland Mexico and consisted of a near-surface westerly sea breeze along with two easterly return flows, one at 2–3 km and another at 5–6 km. Each of these altitudes experienced nighttime cloudiness. The corresponding modulation of the radiative cloud forcing diurnal cycle provided a slight positive feedback upon the sea surface temperature. Two findings were notable. One was an advective warming of over 1°C in the oceanic mixed layer temperature associated with the 13 July surge. The second was the high nighttime cloud cover fraction at 5–6 km, dissipating during the day. These clouds appeared to be thin, stratiform, slightly supercooled liquid-phase clouds. The preference for the liquid phase increases the likelihood that the clouds can be advected farther from their source and thereby contribute to a higher-altitude horizontal moisture flux into the United States.

1. Introduction

Monsoons are fundamentally driven by land–sea heating asymmetries. While the North American Monsoon Experiment (NAME) was well instrumented on land, for logistical reasons observations of the coincident conditions at sea were far fewer. One of the participating research vessels was the Mexican Navy's R/V *Altair*, which positioned itself close to the mouth of the gulf intermediate between Mazatlan and La Paz from 7 July until 12 August.[1] The shipboard measurements

Corresponding author address: Dr. Paquita Zuidema, RSMAS/MPO, 4600 Rickenbacker Cswy., Miami, FL 33149-1098.
E-mail: pzuidema@miami.edu

[1] The other research boats were the R/V *Francisco de Ulloa*, which conducted oceanic transects across the mouth of the gulf in June and August, and the R/V *Puma*, which gathered atmospheric measurements near Mazatlan in August.

DOI: 10.1175/JCLI4089.1

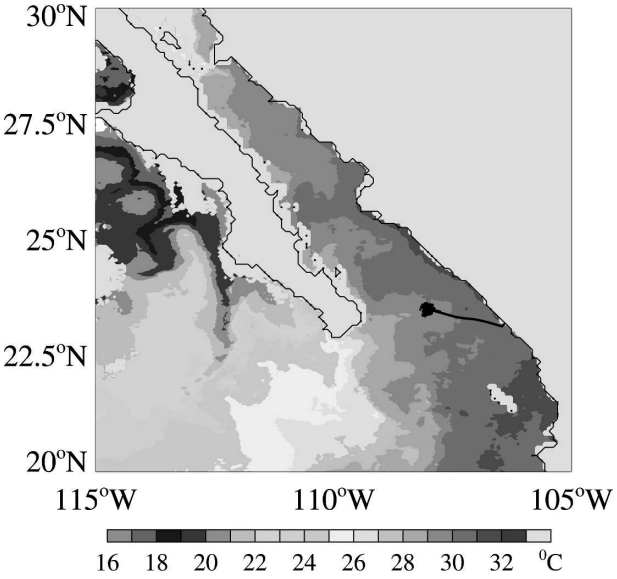

FIG. 1. The 1–8 Jul 2004 mean *Terra* (~1030 LT overpass) MODIS SST, 36-km resolution, with the R/V *Altair* experiment-length ship track superimposed.

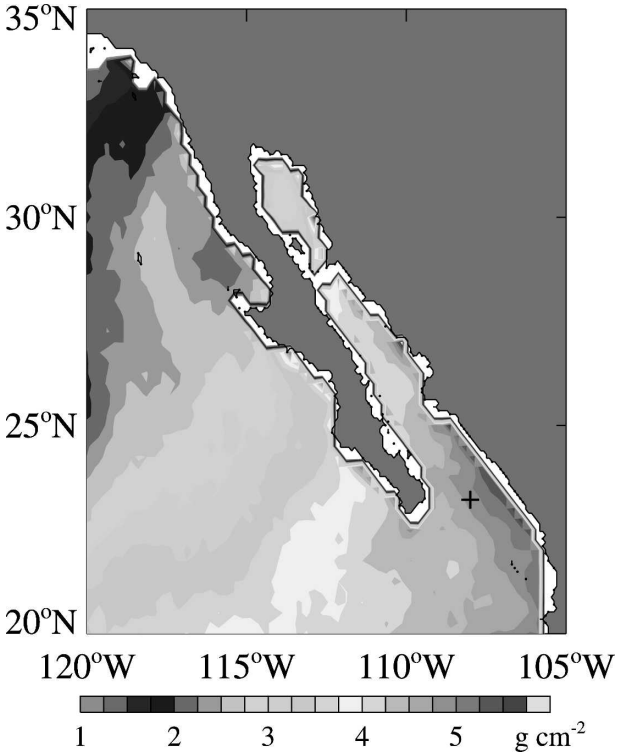

FIG. 2. WVP derived from Special Sensor Microwave Imagery data for 11 Jul 2004. The location of the R/V *Altair* is indicated by a plus sign (+).

contributed to the NAME sounding network, helped assess the contribution of the surface fluxes to the regional meteorology and oceanography, documented the mean and diurnally varying wind flow, and provided a surface-based assessment of the cloud field and boundary layer structure. A preliminary analysis is presented here.

The observational period included a strong gulf surge around 13 July that coincided with the onset of the summer monsoon in southern Arizona. The surge was associated with Tropical Depression Blas to the south and southwest of the *Altair* and an upper-level trough to the northeast of the Gulf of California (GoC) (Johnson et al. 2007). Outflow from Blas helped delay the northward migration of the climatological westerly jet, but after 17 July the upper-level winds at the location of the *Altair* were easterly and stayed that way, signifying an established summer monsoon.

The sea surface temperature (SST) and water vapor path (WVP) fields at the onset of the ship cruise are shown in Figs. 1 and 2, with the *Altair* ship track indicated in Fig. 1. The sea surface temperature gradients in Fig. 1 already make visible a complex regional oceanography. Warmer waters to the east of the *Altair* may reflect a poleward summertime surface current (Lavin et al. 2006) while cooler temperatures to the west of the *Altair* are consistent with westerly wind-driven advection of cooler Pacific surface waters (Bordoni et al. 2004; McNoldy et al. 2006). The atmosphere was moister to the south and east of the *Altair* than north and west of it, and the atmosphere was dry at the north end of the gulf (Fig. 2).

2. Data

The instruments on the *Altair* and their measurements are listed in Table 1. Observations were gathered from 1200 UTC 7 July until 0000 UTC 22 July (leg 1), and from 0000 UTC 27 July until 0000 UTC 12 August (leg 2). The ship was positioned approximately at 23.5°N, 108°W, ~80 km equidistant from land both to the east and the west. Rawindsondes of 2-s vertical resolution were typically launched four times per day, increasing to six times per day during the intensive observation periods. In total, 150 usable soundings of Vaisala type RS80-15G were launched. They have a dry bias in the upper troposphere (Johnson et al. 2007). The sondes used within this paper have not received the quality control procedures documented in Johnson et al. (2007) but visual comparison did not note large discrepancies between the two sonde datasets.

Other atmospheric measurements were gathered by a wind profiler, a ceilometer, and a flux system. The turbulent fluxes presented in this paper were obtained

TABLE 1. R/V *Altair* instruments and measurements.

System	Measurement	Resolution	References
Motion/navigation package	Motion correction for turbulence	20 Hz	Fairall et al. (1997)
Sonic anemo-/thermometer	Direct covariance turbulent fluxes	20 Hz	Fairall et al. (1997)
Infrared fast H_2O/CO_2 sensor	Direct covariance moisture–CO_2 fluxes	20 Hz	Fairall et al. (1997)
Temp and moisture sensors	Bulk turbulent fluxes	20 Hz	Fairall et al. (1996b)
Pyranometer/pyrgeometer	Solar and IR radiative fluxes	1 min	Fairall et al. (1998)
25K Vaisala ceilometer	Cloud-base height	15 s	
915-MHz wind profiler	Winds (up to 3 km)	Half-hourly	Ecklund et al. (1988)
Rawindsondes	Atmospheric temp, RH, and winds	Four to six times daily	Vaisala type RS80-15G
Optical rain gauges	Precipitation rate	1 min	
Sea snake	5-cm-depth ocean temperature	1 min	Fairall et al. (1997)
CTD probe	Ocean temp and salinity profiles	Four times daily	

through bulk aerodynamic methods (Fairall et al. 1996b), but measurements allowing for more accurate direct covariance calculations at a later date were also gathered. Radiative fluxes came from redundant, calibrated pyranometers and pyrgeometers (Fairall et al. 1998). The vertically pointing 915-MHz wind profiler provided continuous profiles of wind in the lower few kilometers at 60- and 110-m resolution, even in the absence of precipitation and below cloud base, by virtue of clear-air refractive index Bragg scattering. Details on motion stabilization and processing of the wind profiler data are given in Fairall et al. (1997). Oceanic temperature and salinity profiles were gathered four times a day to 150-m depth by a conductivity–temperature–depth probe; this probe failed on 31 July. The ocean temperature was measured continuously at 5-cm depth.

3. Atmosphere

The vertically averaged 1000–700-hPa winds and accompanying surface level pressure time series (Fig. 3) highlight the 13 July gulf surge, with winds reaching 12 m s^{-1} and a sea level pressure experiment minimum on 12 July of 1006 hPa. In the context of the SST and WVP fields shown in Figs. 1 and 2, the significance of the southeasterly 13–14 July winds becomes clear, as the winds traveled previously over warmer waters and through a moister atmosphere than that characterizing the *Altair.* Except for the 13 July gulf surge, the lower-troposphere winds were often weak, particularly before 12 July. Occasional enhancements in the southerly winds were associated with gulf surges identified using the index of Bordoni and Stevens (2006).

The experiment-mean rawindsonde wind profiles are contrasted with those from the 13 July gulf surge and from 8 to 11 July in Fig. 4. The experiment-mean wind profiles were weakly southerly at all levels, with a zonal component that was weakly westerly at near-surface levels, becoming easterly above 950 hPa, and strengthening with height. The wind profile from before 12 July is similar to the experiment-mean profile up to 600 hPa, but above that it becomes southwesterly in accord with the premonsoon large-scale flow. The drama of the 13 July gulf surge is revealed in the deep layer of southeasterly winds reaching up to 6 km. These have maximum winds at around 2–3 km (in accord with easterly wave theory) and enhanced easterly flow relative to the previous days at altitudes higher than 5 km.

Mean relative humidity (RH) profiles for the same three time periods are shown in Fig. 5. The near-surface relative humidity was approximately 66%, varying little throughout the experiment, but reaching 73% at the inversion base capping the boundary layer. The boundary layer depth was approximately 350 m in early July, deepening with time and reaching an experiment-mean value of 410 m. This is consistent with the strong surface divergence shown for this region and time period in the Quick Scatterometer (QuikSCAT) winds (Johnson et al. 2007; McNoldy et al. 2006), noted previously in Douglas et al. (1993). Previous observations point to a boundary layer for the northern GoC that is even shallower, with depths of 200–300 m (Badan-Dangon et al. 1991). The inversion depth itself was about 400 m.

All three RH profiles are characterized by increased relative humidity between 450 and 600 hPa. Moisture outflow at the melting level can be a characteristic of tropical convection (e.g., Johnson et al. 1999, and references therein). Two convective sources are thought to have contributed, inferred from the easterly or southeasterly winds prevailing at this altitude. The first, which prevailed regardless of monsoon phase (Fig. 4), was convection over the Sierra Madre Occidental (SMO), occurring even during 8–11 July. The association of SMO convection with melting-level outflow is also noted in (Johnson et al. 2007). Convection was also present to the southeast at times on the SW Mexico mainland (Johnson et al. 2007), and this can contribute outflow during more disturbed periods, such as on 12–

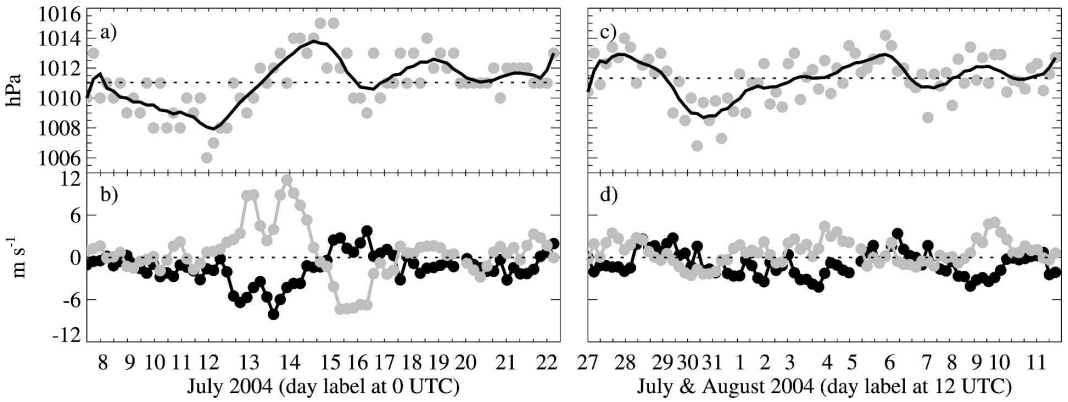

FIG. 3. (a) Surface level pressure as measured by the rawindsondes during leg 1 (solid filled circles and smoothed as a line), and (b) mean 1000–700-hPa rawindsonde meridional and zonal winds (gray and black lines) from 7 until 22 Jul. (c), (d) As in (a), (b) but from 27 Jul until 12 Aug. Note time resolution in all panels varies with the number of rawinsondes per day.

14 July. At pressures below 500 hPa, the difference in the RH values between the different time periods reflects shifts in the prevailing winds; westerly winds are associated with less humidity.

The unique feature of the GoC RH profiles, when compared to typical tropical RH profiles (e.g., Zuidema 1998), is the additional layer of increased moisture at around 2 km apparent in the experiment-mean and premonsoon profiles. It is particularly noticeable in the 8–11 July profile because of the dryness of the air beneath it. Stensrud et al. (1995) discuss a diurnal land breeze at this altitude, consistent with the mostly easterly winds. Over land, the relative humidity at 2-km altitude is typically higher than it is over the gulf (Johnson et al. 2007). The lack of a 2-km moisture layer in the 13 July gulf surge RH profile reinforces the interpretation of a land breeze advecting moisture over the ship during other times.

The distribution of ceilometer-derived cloud-base heights is also trimodal (Fig. 6), with the highest cloud fraction of the three layers occurring at 5–6.5 km (ceilometers only detect cloud bases up to approximately 8 km). Features of the 5–6.5-km cloud layer include a high frequency of cloud bases at temperatures slightly below freezing and a strong diurnal cycle (more obviously seen in Fig. 15), with a nighttime presence and daytime dissipation. The total ceilometer-derived cloud fraction was slightly less during leg 2 than during leg 1, consistent with variations observed in the surface solar and infrared fluxes shown later (see Fig. 8). Cloudiness at 2-km altitude was somewhat episodic. The lowest cloud layer appears to penetrate above the experiment-mean inversion base at times (the ceilometer may also be registering a cloud side), consistent with an increasing RH above the boundary layer and a boundary layer deepening (Fig. 5).

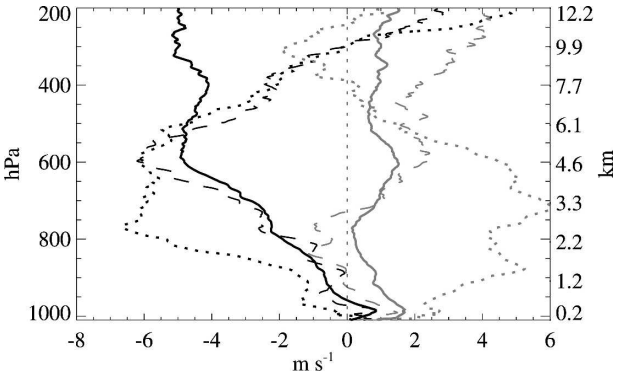

FIG. 4. Experiment-mean, 12–14 Jul mean, and 8–11 Jul mean zonal winds (solid, dotted, and dashed black lines, respectively); similarly for the meridional winds but in gray.

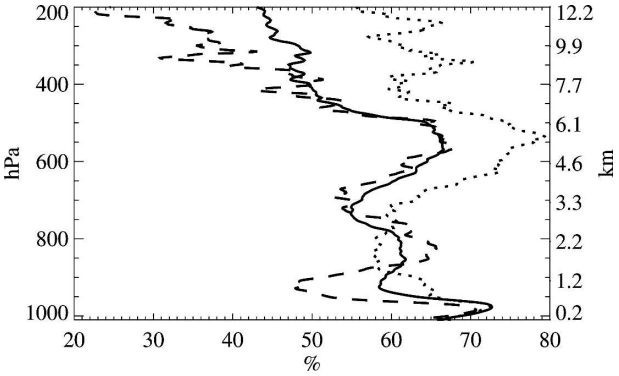

FIG. 5. Experiment-mean, 12–14 Jul mean, and 8–11 Jul mean RH values (solid, dotted, and dashed lines, respectively). Relative humidities at temperatures less than 0°C are with respect to ice.

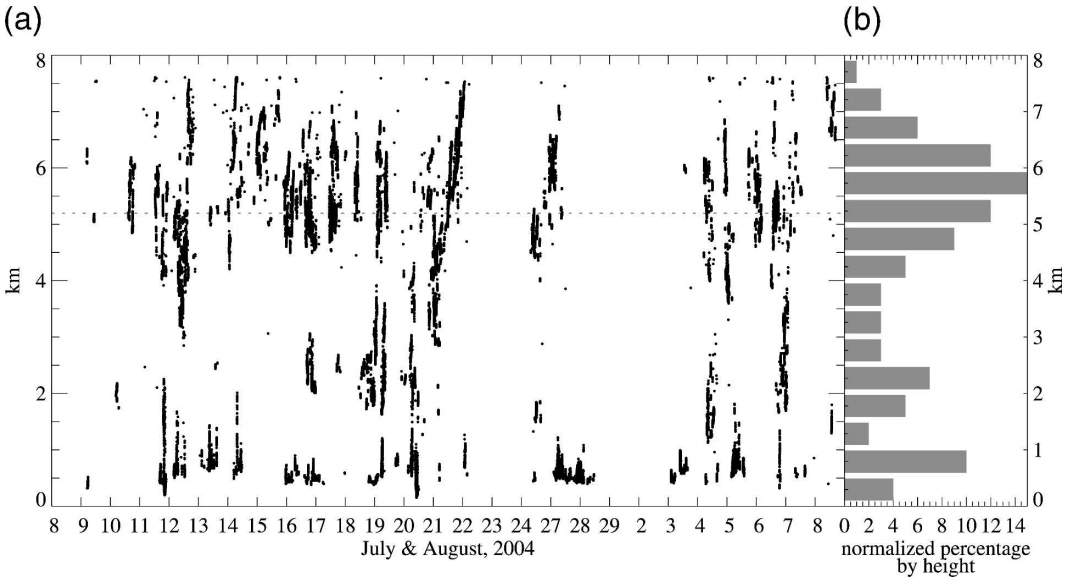

FIG. 6. (a) Time series of ceilometer-derived cloud-base heights, shown only for those days with data. The mean freezing level at 5.2 km is indicated as a dotted line. (b) Experiment-mean vertical distribution of the ceilometer cloud-base heights, expressed as a normalized percentage.

4. Fluxes

The time series of the sea surface temperature at approximately 5-cm depth at the *Altair* is shown in Fig. 7 along with that of the virtual air temperature and the rain rate. Strong diurnal variations are consistently apparent in the SST, with occasional SST increases of 2 K or more in 1 day. This is indicative of solar absorption, with the strongest variations occurring on days with little cloud cover and low wind speeds (e.g., Fairall et al. 1996a).

The experiment-mean SST was 30.3, rising during leg 2 to approach a diurnal average of 31°C. This appears to be 0.5–1.0 K warmer than the mean satellite-derived SST field shown in Fig. 7 of Johnson et al. (2007), more than can be explained by infrared cooling of the surface layer alone. The virtual air temperature was typically less than the SST by 1°–2°C. Downward spikes were associated with precipitation and the subsequent evaporative cooling. The negative air–sea temperature difference contrasts with the positive difference reported for the northern GoC (Badan-Dangon et al. 1991).

Rainfall was infrequent and the accumulated month-long rainfall was light, with an estimated total of 4.2 cm (Fig. 7). The highest rain rate was recorded on 12 July but more rainfall accumulated in August than in July. This is consistent with climatology, which shows an east-to-west progression in precipitation from a maximum over the SMO in July to over the Baja Peninsula in September (Douglas et al. 1993), and with observations of westward-propagating mesoscale vortices over the southern gulf in August (Lang et al. 2007). The 12 July rainfall event occurred at approximately 0600 LT and the August events all occurred between 0200 LT and local noon; the morning preference for GoC con-

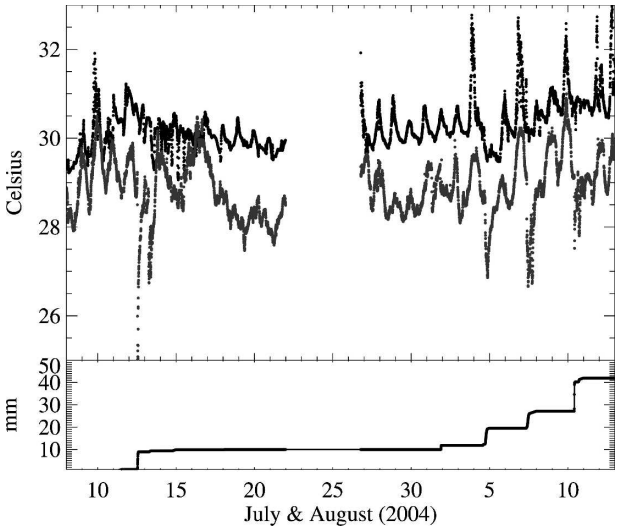

FIG. 7. (top) SST measured at approximately 5-cm depth (black filled circles) and the virtual air temperature measured at the flux tower (gray filled circles). (bottom) Optical rain gauge accumulated rainfall.

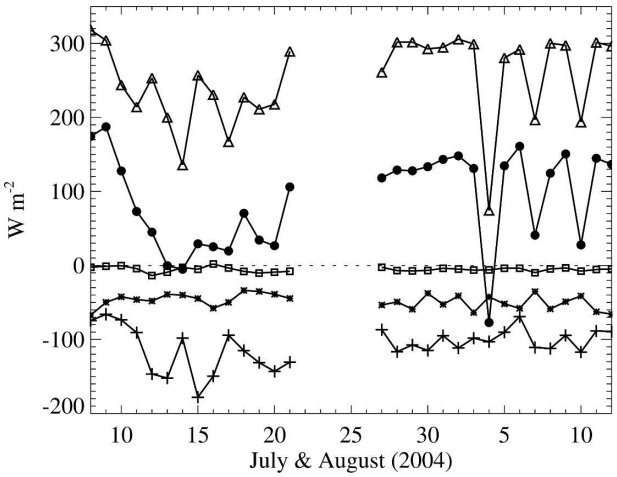

FIG. 8. Time series of daily average surface flux values: net solar (triangles), net IR (asterisks), latent (plus signs), sensible (squares), and net (filled circles). Positive values indicate a surface warming.

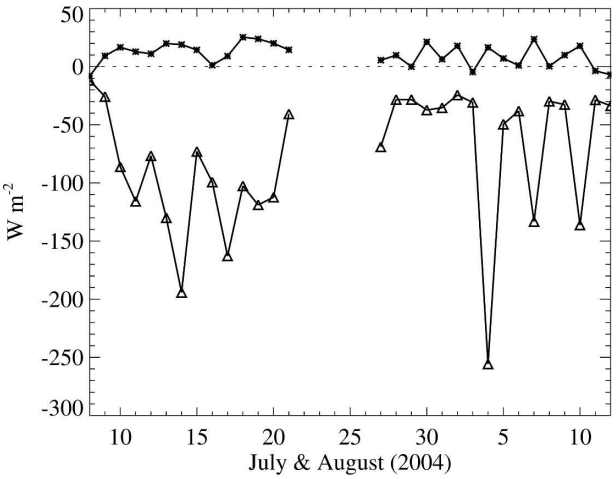

FIG. 9. Time series of the daily averaged surface solar and infrared cloud forcing (triangles and asterisks, respectively). Cloud forcing is calculated as the difference between the net surface radiative flux and the clear-sky surface, with positive values indicating a surface warming attributable to clouds.

vection is consistent with the more comprehensive analysis of s-band dual-polarization Doppler radar (S-Pol) data by Lang et al. (2007).

The daily average surface flux components are shown in Fig. 8; positive values denote a surface warming. The experiment-mean net solar heat flux of 241 W m^{-2} is the dominant warming term, with some days near or above 300 W m^{-2}, indicating little daytime cloud cover. The latent heat flux is the dominant cooling, with an experiment-mean value of -108 W m^{-2} (equivalent to an evaporation rate of 0.16 mm h^{-1}) and a maximum value on 15 July of -180 W m^{-2}. The experiment-mean net heat input was 70 W m^{-2} from the atmosphere into the ocean, consistent with Marinone (2003). On a few occasions (13 and 14 July, and 4 August), the net flux was almost at or below zero, indicating high daytime cloud cover. Apparent from the solar flux values, leg 1 was generally cloudier during the day, while leg 2 contained more daytime cloudiness variability, with both more clear and more deeply cloudy conditions.

The impact of clouds on the surface energy budget is best indicated by the cloud forcing, or the difference in the observed mean radiative flux from the clear-sky flux. The solar cloud forcing is always negative, as clouds decrease the solar radiation at the surface relative to clear-sky conditions, while the infrared cloud forcing is always positive. A time series of the longwave and solar cloud forcing during NAME is shown in Fig. 9, with the clear-sky values calculated from a simple model. The mean solar cloud forcing of -70 W m^{-2} dominates the mean infrared cloud forcing of 10 W m^{-2}, indicating the net cloud effect is a surface cooling.

Table 2 shows the mean surface flux component values measured during NAME and those from other recent field experiments held in suppressed tropical conditions. The fluxes sampled during NAME and other field experiments are comparable to each other. The mean net heat input into the ocean during NAME was on par with undisturbed periods during Tropical Ocean Global Atmosphere Couple Ocean–Atmosphere Response Experiment (TOGA COARE); without clouds, the net heat input would have been approximately 130 W m^{-2}.

5. Ocean

The entrance zone into the GoC lacks a sill, and oceanic depths at locations near the *Altair* can reach 3000 m (Lavin and Marinone 2003). As a consequence, the mouth of the GoC is open to far-reaching influences from the tropical Pacific as well as from the gulf itself. This is evident even in the one-point oceanic profiles taken at the *Altair* (Fig. 10). Experiment-mean profiles of temperature, salinity, and density, along with those from 8 and 30 July, show the oceanic mixed layer had a mean temperature near 30°C and a mean depth of approximately 20 m that changed little throughout the experiment. The themocline weakened slightly with time, with temperatures below the thermocline increasing more dramatically than those above it. A near-surface layer of 1–2-m thickness was slightly fresher than the water beneath it, possibly reflecting westerly wind-driven advection of fresher waters. Occasionally a layer of fresher water was present just below the mixed layer, but this is not evident in the profiles shown here.

TABLE 2. Mean surface flux components from recent field experiments (W m^{-2}). Positive values correspond to a surface warming.

Experiment	Net shortwave	Net longwave	Sensible	Latent	Net
TOGA COARE[a] (undisturbed)	222	−58	−7	−89	65
JASMINE[b] (preonset)	260	−49	−5	−115	90
Nauru99[c]	216	−54	−5	−123	33
NAME height	241	−57	−5	−108	70

[a] Reproduced from Fairall et al. (1996b).
[b] Joint Air–Sea Monsoon Interaction Experiment (Webster et al. 2002).
[c] Post et al. (1997).

The mixed layer freshening with time contrasts with the dominance of evaporation over precipitation (approximately 120 mm in 1 month) and implies either advection or entrainment from below is taking place. A salinity–temperature classification applied to the *Altair* data suggests an advection of tropical surface waters was occurring (Castro et al. 2006).

The mixed layer temperature increased over 1°C from 10 to 12 July (Fig. 11). After attaining a daily mean temperature of 30.5°C on 12 July, the mixed layer temperature decreased slightly thereafter, with strong diurnal variations. No discernible salinity change was associated with the strong warming. Toward the end of July, the mixed layer freshened significantly, but it is not known if the cause is precipitation (Fig. 7) or advection.

A rise of 1.2°C by a 20-m-deep mixed layer over 2.5 days requires a heat flux of about 215 W m^{-2}. Given that the net surface heat flux was around zero on 12–13 July (Fig. 8), it is likely that most of the mixed layer warming, and possibly the mixed layer diurnal temperature oscillations, occurring up to 18 July can be attributed to oceanic heat transport. This is consistent with Castro et al. (1994) and Mascarenhas et al. (2004), who report an input of heat from the Pacific Ocean into the GoC from late spring until midsummer. Marinone (2003) also mention a dominance of the horizontal oceanic heat transport at the mouth of the GoC over the surface heat flux in determining the seasonal heat and salinity balances. What is unusual, however, is the large extent one event, the 13 July gulf surge, played in raising the mixed layer temperature.

6. Diurnal cycle

Details of the land–sea breeze circulation in the GoC depend strongly on location, evident in the more comprehensive spatial analyses of Gille et al. (2005) and particularly McNoldy et al. (2006). The *Altair* was located approximately 80 km from land both to the east and to the west. At this location the diurnal cycle in the near-surface winds, as measured by a sonic anemometer at approximately 15-m altitude, was much more influenced by the mainland of Mexico than by Baja California (Fig. 12), also seen in McNoldy et al. (2006). The experiment-mean winds show westerly (eastward) flow after local noon with a broad peak from 1500 LT until midnight. This is consistent with simple land-breeze theory and with an analysis of buoy data examining the dependence on distance from the coast of

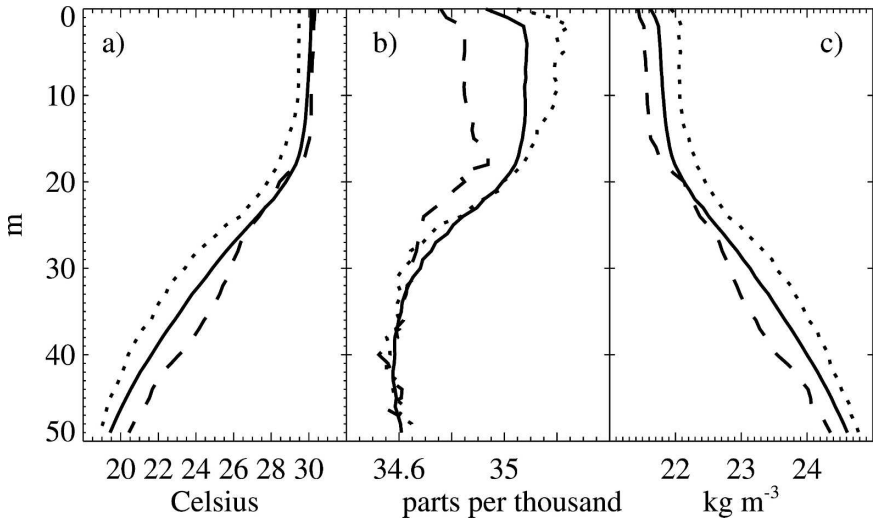

FIG. 10. (a) Experiment-mean oceanic temperature, (b) salinity, and (c) density profiles (solid line) and those from 8 (dotted line) and 30 Jul (dashed line).

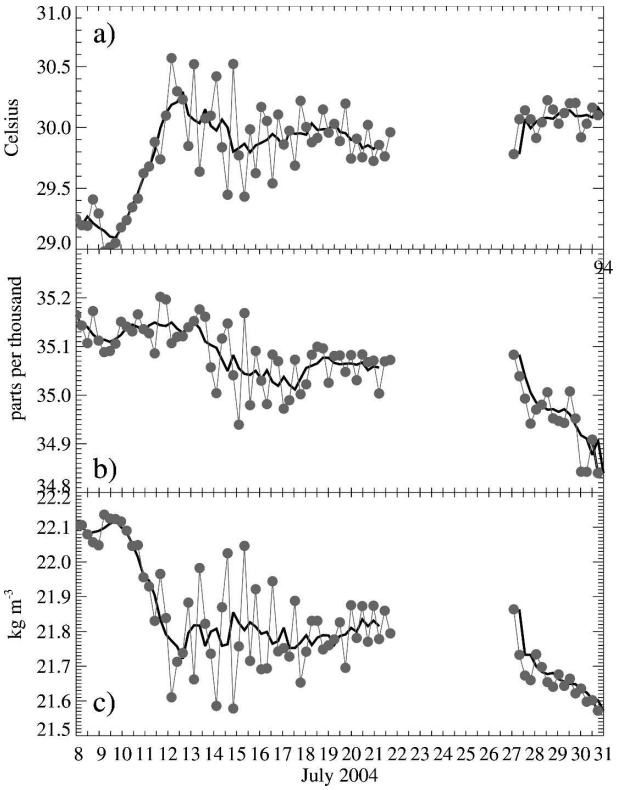

FIG. 11. Upper-oceanic 20-m layer: (a) temperature, (b) salinity, and (c) density measurements (solid filled circles and a smoothed line).

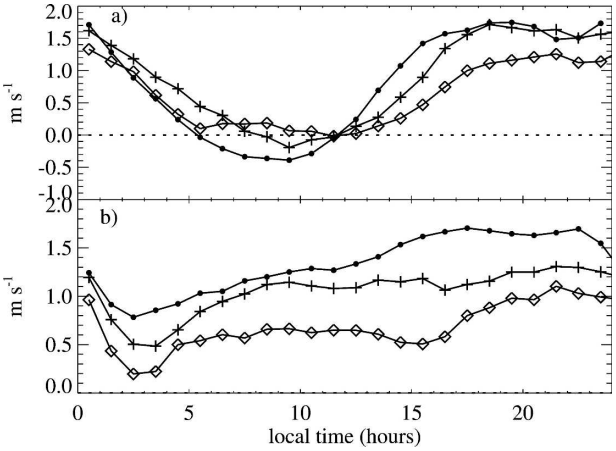

FIG. 12. (a) Zonal wind diurnal cycle from the sonic anemometer (black filled circles), and the wind-profiler data for the lowest gate at 100- (diamonds) and 60-m resolution (plus signs). (b) As in (a) but for meridional winds.

southern California (Lerczak et al. 2001), suggesting only a subtle influence of Baja California upon the land–sea-breeze circulation at this location and time. The near-surface wind diurnal cycle inferred from the wind profiler is similar, albeit more muted, to that derived from the sonic anemometer (Fig. 12). The experiment-mean near-surface meridional winds were southerly irrespective of time of day, which contrasts with the model depiction of Berbery (2001). The mouth of the gulf is characterized by a surface wind divergence (Bordoni et al. 2004), however, and near-surface meridional winds slightly to the south of the *Altair* may well be northerly.

The diurnal cycle varied during the experiment (Fig. 13). The experiment-mean diurnal cycle shown in Fig. 12 is reproduced as a wind hodograph in Fig. 13a. Early on the near-surface winds were westerly irrespective of time of day, with a maximum that occurred around 2000 LT (Fig. 13b). The 13–14 July time period contained a much stronger mean easterly component, with a shift to an earlier zonal wind minimum and maximum, and also contained a pronounced meridional wind diurnal cycle (Fig. 13c). The strong nighttime southerlies are consistent with the presence of a southerly nighttime low-level jet in the northern GoC (Douglas 1995; Johnson et al. 2007; Stensrud et al. 1997). On days other than 12–14 July, however, a nighttime maximum was not evident in the meridional wind, which is also consistent with previous findings that a low-level nocturnal jet is more characteristic of the northern GOC than the southern GoC (Douglas et al. 1993). In August, a slight bimodality in the meridional winds was apparent and the onshore westerly flow was more limited to before 2000 LT. Convective processes and boundary layer flow appear to have been more complex in August than July, with occasional offshore land–sea-breeze convergence leading to convection, and an east-to-west mesoscale vortex propagation. These are discussed by Lang et al. (2007) and relating them to the *Altair* observations will require more analysis. The variation with time in the diurnal cycle phasing apparent in Fig. 13 could bias diurnal cycle inferences drawn from QuikSCAT winds alone, as these are only routinely available at 0600 and 1800 LT.

The wind profiler provides a view of the daily cycle in winds up to 3 km in altitude, as is shown in Fig. 14 for the experiment mean along with a measure of the directional constancy. A directional constancy value of one indicates the direction was constant in time, and a value of zero indicates the direction was either evenly divided between two opposing directions, or among all directions (Hartten et al. 2007, manuscript submitted to *J. Climate*, hereafter HKZ). The midafternoon to midnight near-surface westerly flow (Fig. 13a) extends up to a maximum of about 750-m altitude at 1600 LT, decreasing in height thereafter. A nighttime near-surface land breeze, evident in the wind profiler diurnal cycle at Estacion Obispo (on land, at 24.28°N,

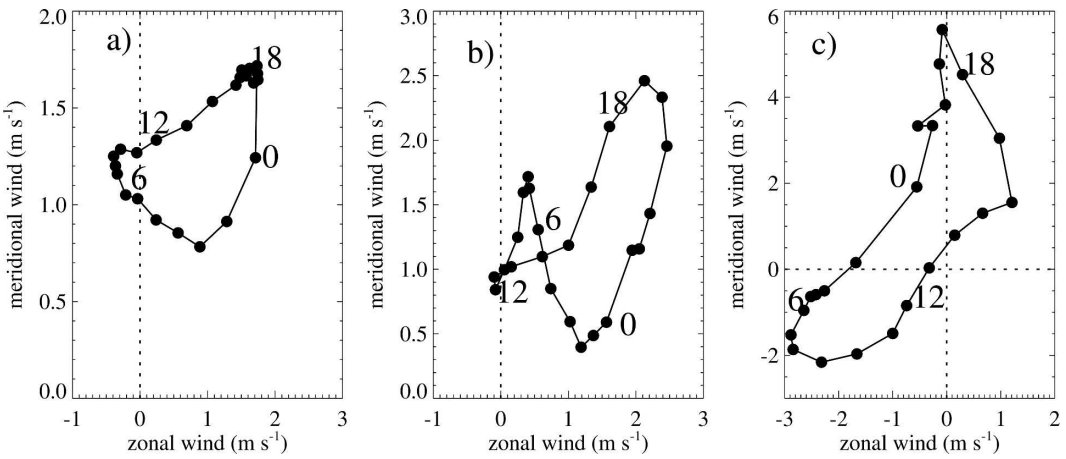

FIG. 13. Diurnal cycle sonic anemometer wind hodographs for (a) experiment mean, (b) 8–11 Jul mean, and (c) 13–14 Jul mean. Numbers indicate local time.

107.16°W) is not evident in the *Altair* daily cycle (HKZ). The easterly return flow at 2–3 km thought responsible for enhanced RH over the gulf (Fig. 5) occurs from 0200 LT until almost noon, extending downward in time. It is most consistent and strongest at around 0900 LT, with wind speeds of around 3 m s^{-1}.

The rawindsondes resolve a diurnal cycle in relative humidity and winds with a greater vertical extent and poorer temporal resolution than the wind profiler or sonic anemometer. These are shown in Fig. 15 along with the fraction of ceilometer cloud-base heights as a function of height and time of day. At near-surface levels the nighttime increase in relative humidity is accompanied by low clouds. The nighttime 2-km easterly flow is also accompanied by an increase in RH, with the cloud occurrence between 0600 and 0900 LT correlating well with the wind-profiler diurnal cycle and less so with the RH maximum.

The most striking feature in Fig. 15 is the consistent easterly flow at 500 hPa accompanied by nighttime cloud cover. Clouds at this level composed the highest cloud fraction within the ceilometer dataset (see also Fig. 6). Both Douglas et al. (1993) and Schmitz and Mullen (1996) discuss low-level GoC moisture that is advected upward by SMO convection, outflowing back to the gulf at higher altitudes, and mention that it is more pronounced at the southern end of the GoC; this study shows that the outflow is characterized by cloudiness as well as moisture.

The experiment-mean diurnal cycle in the surface infrared cloud forcing reflects the diurnal cycle observed in the ceilometer-derived cloud coverage. The experiment-mean diurnal cycle in the surface infrared cloud forcing is a maximum at 0100 LT (19 W m^{-2}), falls to half this at 0900 LT, and reaches a minimum of 1 W m^{-2} at 1500 LT. Thus, the cloudiness diurnal cycle serves to enhance the net radiative flux into the ocean, by reducing the nighttime oceanic infrared heat loss yet still allowing daytime oceanic solar absorption.

7. Summary and discussion

The experiment-mean findings include the following:

- a boundary layer depth of approximately 410 m, deepening with time from an initial value of 350 m;
- a trimodal atmospheric moisture and cloudiness distribution, with enhanced moisture and clouds within the boundary layer, at 2–3 km (associated with an elevated land–sea-breeze circulation) and at 5–6 km (associated with outflow from SMO convection and at times with outflow from convection to the SE of the *Altair*);
- total accumulated rainfall of 4.2 cm, with most of it occurring in August;
- a net heat input from the atmosphere into the ocean of 70 W m^{-2}, where the net solar absorption was 241 W m^{-2} and the surface latent heat flux was −108 W m^{-2}, equivalent to a mean evaporation rate of 0.16 mm h^{-1}; these values are comparable to those from other recent field experiments in suppressed tropical conditions;
- an almost consistently southerly near-surface meridional wind component; and
- an oceanic mixed layer depth of about 20 m, which warmed and also freshened throughout the experiment, despite a local dominance of evaporation over precipitation. The depth changed little, though the thermocline weakened slightly.

The boundary layer was deeper (by over 100 m) compared to observations of the northern GoC boundary

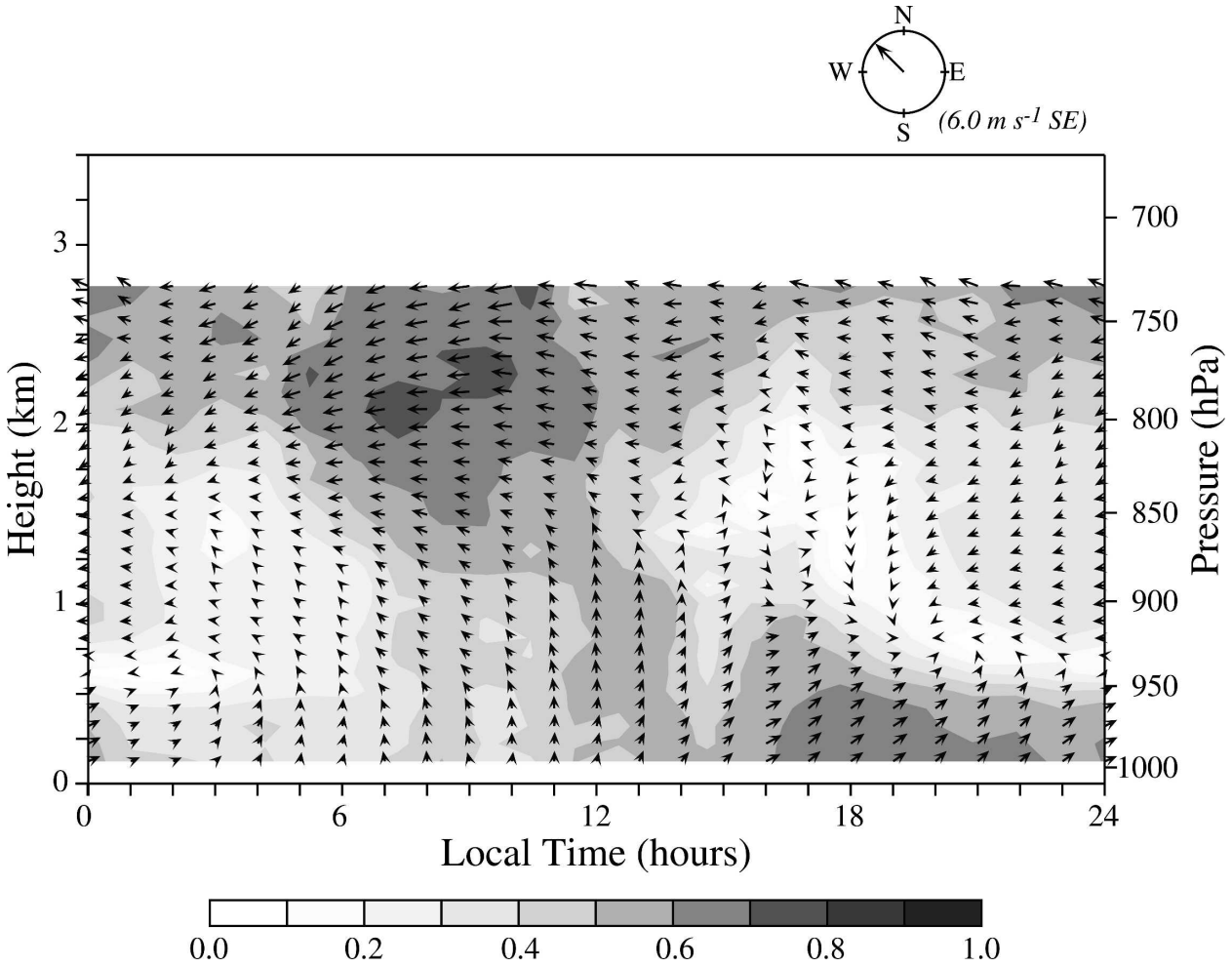

FIG. 14. Experiment-mean diurnal cycle in wind-profiler-derived vector winds as a function of local time, together with their directional constancy (shaded). A 6 m s^{-1} southeasterly reference vector is shown above.

layer, and, in contrast to the northern GoC, the air–sea temperature difference was negative rather than positive (Badan-Dangon et al. 1991).

The observational time period of the *Altair* included a strong gulf surge around 13 July associated with the onset of the southwest U.S. monsoon. The period of 8–11 July was characterized by light winds and little daytime cloud cover. Decreased surface pressures on 11 July were followed by southeasterly winds reaching 12 m s^{-1} (Fig. 3). The high winds encouraged high surface latent heat fluxes (120–180 W m^{-2}); these did not increase the surface RH but did increase the depth of the boundary layer. The cloud cover fraction was high and the net surface fluxes approached zero. A nighttime southerly wind maximum coincided with the nocturnal jet more commonly observed in the northern GoC. Some precipitation occurred on 12 July at about 0600 LT, and atmospheric sublimation and evaporation of precipitation were also apparent in the attenuation of the ceilometer reflectivites.

Observations of the diurnal cycle include the following:

- The near-surface winds were westerly after local noon, with a broad peak from 1500 LT until midnight. This suggests that mainland Mexico is the main influence upon the diurnal cycle at this location and time period. A diurnal cycle in the meridional component was only evident during the 13 July gulf surge.
- No near-surface land breeze off of the mainland Mexico was observed.
- The diurnal cycle in the near-surface winds varied throughout the experiment, which may have ramifications for diurnal cycle inferences drawn from QuikSCAT winds alone.
- The near-surface westerly winds reached a height of 750 m at around 1400 LT, decreasing in height thereafter.

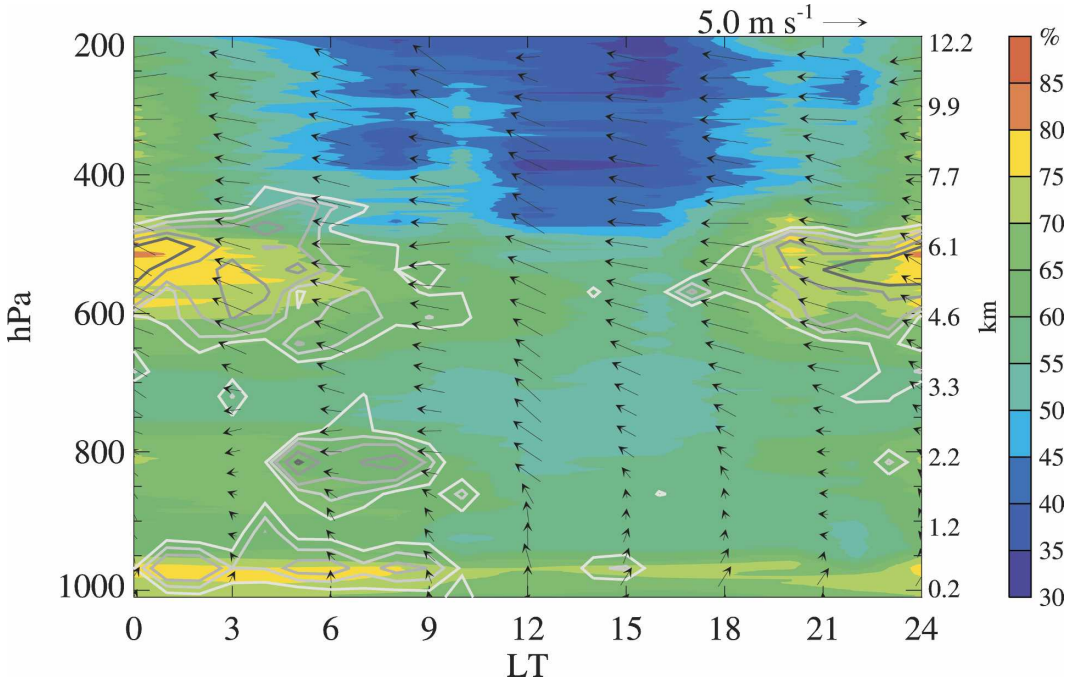

FIG. 15. Mean diurnal cycle in rawinsonde RH as a function of local time, along with the diurnal-mean ceilometer cloud-base height fraction and the diurnal-mean zonal and meridional rawinsonde winds. The ceilometer cloud bases are binned hourly in 500-m-height bins, with the contour levels indicated at 2%, 3%, 4%, 6%, and 8% of the total. A 5 m s^{-1} reference vector is shown above.

- An easterly return flow was evident between 2 and 3 km from 0200 LT until noon, with the strongest and most consistent flow at around 0900 LT, corresponding to a wind speed of around 3 m s^{-1}.
- The rawindsondes documented an easterly or southeasterly flow at 5–6 km, lasting from 1800 LT until 0900 LT the next day with wind speeds reaching 5 m s^{-1}. The associated nighttime cloud cover formed the largest cloud fraction within the ceilometer data.
- All three cloud layers have nighttime maxima, with little daytime presence. The diurnal cycle in the infrared cloud forcing is consistent with this, with a maximum of 19 W m^{-2} at 0100 LT and a minimum of 1 W m^{-2} at 1500 LT. The diurnal modulation in the infrared cloud forcing diurnal provides a slight positive feedback upon the ocean surface temperature, by reducing nighttime heat loss yet encouraging daytime solar absorption.

Two findings of this study are unusual. One is the impact of the 13 July surge upon the sea surface temperature and oceanic mixed layer temperature: an increase in both of over 1°C, equivalent to a heat input of about 215 W m^{-2} spanning 2.5 days. Given that the net surface heat flux approached zero during 13–14 July, the temperature increases can only be explained by horizontal oceanic advection. Horizontal oceanic heat transport is known to be important to the southern GoC heat balance (Castro et al. 2006; Lavin and Marinone 2003; Lavin et al. 2006; Marinone 2003; Mascarenhas et al. 2004), but the impacts of individual transient surges have not received much attention. This coincidence of the increase in GoC SST with an atmospheric moisture flux into southwestern United States, that is, two independent responses to the same large-scale circulation change, may help explain the correlation observed between GoC SST and U.S. monsoonal moisture despite the small basin size of the GoC (e.g., Mitchell et al. 2002).

The second unusual finding is the documentation of the high nighttime cloud fraction at 5–6 km. Some of this may reflect outflow from convection occurring on the mainland to the southeast of the *Altair* (Johnson et al. 2007). Another source is SMO convection. Douglas et al. (1993) and Schmitz and Mullen (1996) both discuss the upward advection of low-level GoC moisture through SMO convection, with outflow at higher levels back over the gulf, and mention it should be particularly pronounced at the southern end of the gulf. The association of these outflows with cloudiness at 5–6 km has not previously been documented. It appears likely that these clouds are liquid rather than ice, despite cloud bases at temperatures below freezing. The liquid

phase is consistent with more definite lidar remote sensing results for similar midlevel clouds (Young et al. 2000), with a lack of active ice nuclei between the temperatures of 0° and −10°C (Pruppacher and Klett 1978), with the hard detection of a cloud base by the ceilometer, and with visual observations of a thin, stratiform structure.

One ramification of the liquid phase is that the thin cloud is more easily maintained through infrared radiative cloud-top cooling and cloud-base warming, then dissipating during the day through solar absorption, thereby providing a positive radiative feedback to the ocean temperatures below. Another ramification of the liquid phase is that the condensate will remain concentrated at the 5–6-km level, whereas precipitating ice would serve to advect moisture downward. The clouds can be advected farther from the source despite their thinness, and may contribute a higher-altitude horizontal moisture flux into the United States.

The limitations of this preliminary analysis provide several directions for future work. High-resolution modeling studies are needed to explore the role of the 5–6-km moisture. There is evidence of evaporation and/or sublimation in the ceilometer backscattered intensities; these need to be quantified to understand their contribution to the moisture and energy budget and compared to model values. The air–sea characteristics of surges other than the 13 July surge have not been investigated. The evolution of the atmospheric boundary layer also remains to be investigated. This includes its relationship to the large-scale surface divergence, which is thought to vary diurnally in response to the land–sea breeze.

On a larger scale, the *Altair* measurements are only point values from within a complex setting and more spatial analysis and modeling are required to understand the relationship between local and advective processes. The August time period in particular has been ignored here; the regional dynamics appear to have been more complex then than in July, with convective systems traveling as much across the gulf as along it (Lang et al. 2007). It would be useful to more fully elucidate the oceanic manifestation of gulf surges, including evaluating how far north the oceanic advection of warm waters can be carried, toward addressing the relationship between the GoC ocean and atmosphere. Perhaps more fully coupled regional ocean–atmosphere models can address this, although these would probably require buoy measurements to help constrain them.

Acknowledgments. The *Terra* MODIS level 3 SSTs shown in Fig. 1 were obtained from the Physical Oceanography Distributed Active Archive Center (PO.DAAC) at NASA JPL in Pasadena, California (information online at http://podaac.jpl.nasa.gov). Dr. Gary Wick supplied the Special Sensor Microwave Imagery water vapor path data shown in Fig. 2. Other scientists and engineers contributing to the success of the cruise include Javier Zavala-Garay from the University of Miami; Brenda Dolan, Gustavo Pereira, and Andrea Saunders from Colorado State University; Scott Abbott and Sergio Pezoa from NOAA; and Allen White and Dave White for processing of the wind profiler data. The Mexican Navy personnel are gratefully acknowledged, in particular Captain Gustavo Montarde and translator F. Gonzalez-Belmonte. Miguel Lavin and Ruben Castro helped educate the first author on the GoC oceanography. This work was supported by the NOAA Office of Global Programs, in collaboration with the Navy of Mexico. We thank the many whose dedication made the North American Monsoon Experiment possible.

REFERENCES

Badan-Dangon, A., C. E. Dorman, M. A. Merrifield, and C. D. Winant, 1991: The lower atmosphere over the Gulf of California. *J. Geophys. Res.,* **96,** 877–896.

Berbery, E. H., 2001: Mesoscale moisture analysis of the North American monsoon. *J. Climate,* **14,** 121–137.

Bordoni, S., and B. Stevens, 2006: Principal component analysis of the summertime winds over the Gulf of California: A gulf surge index. *Mon. Wea. Rev.,* **134,** 3395–3414.

——, P. E. Ciesielski, R. H. Johnson, B. D. McNoldy, and B. Stevens, 2004: The low-level circulation of the North American monsoon as revealed by QuikSCAT. *Geophys. Res. Lett.,* **31,** L10109, doi:10.1029/2004GL020009.

Castro, R., M. Lavin, and P. Ripa, 1994: Seasonal heat balance in the Gulf of California. *J. Geophys. Res.,* **99,** 3249–3261.

——, R. Durazo, A. Mascarenhas, C. Collins, and A. Travina, 2006: Thermohaline variability and geostrophic circulation in the southern portion of the Gulf of California. *Deep-Sea Res.,* **53,** 188–200.

Douglas, M. W., 1995: The summertime low-level jet over the Gulf of California. *Mon. Wea. Rev.,* **123,** 2334–2347.

——, R. A. Maddox, K. Howard, and S. Reyes, 1993: The Mexican monsoon. *J. Climate,* **6,** 1665–1677.

Ecklund, W. L., D. A. Carter, and B. B. Balsley, 1988: A UHF wind profiler for the boundary layer: Brief description and initial results. *J. Atmos. Oceanic Technol.,* **5,** 432–441.

Fairall, C. W., E. F. Bradley, J. S. Godfrey, G. A. Wick, J. B. Edson, and G. S. Young, 1996a: Cool-skin and warm-layer effects on sea surface temperature. *J. Geophys. Res.,* **101,** 1295–1308.

——, ——, D. P. Rogers, J. B. Edson, and G. S. Young, 1996b: Bulk parameterization of air–sea fluxes for TOGA-COARE. *J. Geophys. Res.,* **101,** 3747–3767.

——, A. B. White, J. B. Edson, and J. E. Hare, 1997: Integrated shipboard measurements of the marine boundary layer. *J. Atmos. Oceanic Technol.,* **14,** 338–359.

——, P. O. Persson, E. F. Bradley, R. E. Payne, and S. Anderson, 1998: A new look at calibration and use of Eppley precision

infrared radiometers. Part I: Theory and application. *J. Atmos. Oceanic Technol.,* **15,** 1229–1242.

Gille, S., S. L. Smith, and N. M. Statom, 2005: Global observations of the land breeze. *Geophys. Res. Lett.,* **32,** L05605, doi:10.1029/2004GL022139.

Johnson, R. H., T. Rickenbach, S. A. Rutledge, P. Ciesielski, and W. Schubert, 1999: Trimodal characteristics of tropical convection. *J. Climate,* **12,** 2397–2418.

——, P. E. Ciesielski, B. McNoldy, P. Rogers, and R. Taft, 2007: Multiscale variability of the flow during the North American Monsoon Experiment. *J. Climate,* **20,** 1628–1648.

Lang, T. J., D. A. Ahijevych, S. W. Nesbitt, R. E. Carbone, S. A. Rutledge, and R. Cifelli, 2007: Radar-observed characteristics of precipitating systems during NAME 2004. *J. Climate,* **20,** 1713–1733.

Lavin, M., and S. Marinone, 2003: An overview of the physical oceanography of the Gulf of California. *Nonlinear Processes in Geophysical Fluid Dynamics,* O. U. Velasco Fuentes et al., Eds., Kluwer Academic, 173–204.

——, E. Beier, V. G. J. Gomex-Valdex, and J. Garcia, 2006: On the summer poleward coastal current of SW México. *Geophys. Res. Lett.,* **33,** L02601, doi:10.1029/2005GL024686.

Lerczak, J., M. Herdershott, and C. Winant, 2001: Observations and modeling of coastal internal waves driven by a diurnal sea breeze. *J. Geophys. Res.,* **106,** 19 715–19 729.

Marinone, S., 2003: A three-dimensional model of the mean and seasonal circulation of the Gulf of California. *J. Geophys. Res.,* **108,** 3325, doi:10.1029/2002JC001720.

Mascarenhas, A., R. Castro, C. Collins, and R. Durazo, 2004: Seasonal variation of geostrophic velocity and heat flux at the entrance to the Gulf of California, Mexico. *J. Geophys. Res.,* **109,** C07008, doi:10.1029/2003JC002124.

McNoldy, B. D., P. E. Ciesielski, and R. H. Johnson, 2006: Diurnal cycle of sea surface winds and temperatures during the 2004 North American Monsoon Experiment. Preprints, *27th Conf. on Hurricanes and Tropical Meteorology,* Monterey, CA, Amer. Meteor. Soc., CD-ROM, P2.2.

Mitchell, D. L., D. Ivanova, R. Rabin, T. Brown, and K. Redmond, 2002: Gulf of California sea surface temperatures and the North American monsoon: Mechanistic implications from observations. *J. Climate,* **15,** 2261–2281.

Post, M. J., and Coauthors, 1997: The Combined Sensor Program: An air–sea science mission in the central and western Pacific Ocean. *Bull. Amer. Meteor. Soc.,* **78,** 2797–2815.

Pruppacher, H. R., and J. D. Klett, 1978: *Microphysics of Clouds and Precipitation.* Kluwer Academic, 962 pp.

Schmitz, J. T., and S. L. Mullen, 1996: Water vapor transport associated with the summertime North American monsoon as depicted by ECMWF analyses. *J. Climate,* **9,** 1621–1634.

Stensrud, D. J., R. L. Gall, S. L. Mullen, and K. W. Howard, 1995: Model climatology of the Mexican monsoon. *J. Climate,* **8,** 1775–1793.

——, ——, and M. K. Nordquist, 1997: Surges over the Gulf of California. *Mon. Wea. Rev.,* **125,** 417–437.

Webster, P., and Coauthors, 2002: The JASMINE pilot study. *Bull. Amer. Meteor. Soc.,* **83,** 1603–1630.

Young, S. A., C. M. R. Platt, R. T. Austin, and G. R. Patterson, 2000: Optical properties and phase of some midlatitude, midlevel clouds in ECLIPS. *J. Appl. Meteor.,* **39,** 135–153.

Zuidema, P., 1998: The 600–800-mb minimum in tropical cloudiness observed during TOGA COARE. *J. Atmos. Sci.,* **55,** 2220–2228.